Configuration Entropy Effect on Temperature Coefficient of Redox Potential of *P*2-Na_xCoO_2

Yuya Fukuzumi[1], Yoyo Hinuma[2], and Yutaka Moritomo[1,3,4]

[1] Graduate School of Pure and Applied Sciences, University of Tsukuba, Tsukuba, 305-8571, Japan

[2] Center for Frontier Science, Chiba University, Chiba, 263-8522, Japan

[3] Faculty of Pure and Applied Sciences, University of Tsukuba, Tsukuba, 305-8571, Japan

[4] Tsukuba Research Center for Energy Materials Science (TREMS), University of Tsukuba, Tsukuba, 305-8571, Japan

E-mail: moritomo.yutaka.gf@u.tsukuba.ac.jp

Abstract. The temperature coefficient (α) of redox potential (V) is a significant material parameter that coverts thermal energy into electric energy. In this paper, we determined α of $P2$-type Na_xCoO_2 against the Na^+ concentration (x). The solid component ($\alpha_{\rm solid}$) of α scatters from -0.18 mV/K to 0.64 mV/K. The phase separation (PS) model cannot reproduce the x-dependence even qualitatively. We interpreted the unexpected disagreement in terms of the residual configuration entropy in the pseudo-disordered region between the Na^+ ordered phases.

Submitted to: *Jpn. J. Appl. Phys.*

1. INTRODUCTION

A new energy harvesting technology, which converts waste heat near room temperature and/or human body heat to electric energy at low cost and high efficiency, is required for a "smart" society. Recently, several researchers[1, 2, 3, 4, 5] reported that a thermocell that uses the difference in the thermal coefficient ($\alpha = \mathrm{d}V/\mathrm{d}T$) of the redox potential (V) between the anode (α_{anode}) and cathode ($\alpha_{\mathrm{cathode}}$) materials can convert the cell temperature (T_{cell}) into the electric energy. The thermocell can produce electric energy in the thermal cycle between low (T_{L}) and high (T_{H}) temperatures, making in sharp contrast with the semiconductor-based thermoelectric device.[6] In the warming process, the redox potentials of the anode and cathode change by $\alpha_{\mathrm{anode}}\Delta T$ and $\alpha_{\mathrm{cathode}}\Delta T$, respectively. Then, we expect a thermally induced change in the cell voltage (V_{cell}) as large as $(\alpha_{\mathrm{cathode}} - \alpha_{\mathrm{anode}})\Delta T$. In other words, electric energy is thermally stored in the thermocell. The stored electric energy can be extracted by the discharge process at T_{H}. Similarly, during the cooling process, the redox potentials of the anode and cathode change by $-\alpha_{\mathrm{anode}}\Delta T$ and $-\alpha_{\mathrm{cathode}}\Delta T$, respectively. The stored electric energy can be extracted by the discharge process at T_{L}. For example, Shibata *et al.*[5] fabricated a thermocell consisting of two types of cobalt Prussian blue analogues (Co-PBAs) with different α values. The thermocell produces electric energy with high thermal efficiency ($\eta = 1$ %) between T_{L} (= 295 K) and T_{H} (= 323 K). This type of thermocell expands the application region of the battery materials from energy storage to energy conversion. To realize a new energy harvesting device, exploration of high-$|\alpha|$ material is indispensable.

From a thermodynamically point of view, α is equivalent to $\frac{1}{e}\Delta S$, where e and ΔS are the elementary charge (> 0) and the differences in entropy (S) of the system before and after Na^+ insertion. Furthermore, ΔS can be divided into the components due to electrode solid material ($\Delta S_{\mathrm{solid}}$) and electrolyte ($\Delta S_{\mathrm{electrolyte}}$).[7] Recently, Fukuzumi *et al.*[8] investigated α of $LiFePO_4$, which is one of the most prototypical intercalation compounds used as a cathode for lithium-ion secondary batteries (LIBs). Importantly, Li_xFePO_4 shows phase separation (PS) into $FePO_4$ and $LiFePO_4$ during the Li^+ intercalation process as

$$FePO_4 + Li^+ + e^- \rightarrow LiFePO_4. \tag{1}$$

Actually, α (= 0.9 mV/K) is nearly independent of the Li^+ concentration (x). Within the framework of the PS model, $\Delta S_{\mathrm{solid}}$ is simply expressed as $S(LiFePO_4) - S(FePO_4)$. Fukuzumi *et al.* further confirmed that the experimentally-obtained α (= 0.9 mV/K) is quantitatively reproduced by $\Delta S_{\mathrm{solid}}$ evaluated by first principles calculations and $\Delta S_{\mathrm{electrolyte}}$. Other than $LiFePO_4$, α values are reported for Prussian blue analogues.[4, 9]

Among battery materials, Na_xCoO_2 with $P2$-type structure ($P6_3/mmc$, $Z = 2$) is most intensively investigated.[10, 11, 12, 13, 14, 15] In the $P2$-type structure, the edge-sharing CoO_2 layer and Na sheet are alternately stacked (Fig. 1). The close-packed oxygen sheets stack as AB|BA, in a sharp contrast to the AB|CA|BC stacking in the α-$NaFeO_2$ structure. As a result, the Na site is surrounded by the oxygen triangular prism. The compound shows a discharge capacity of 130 mAh/g and an average

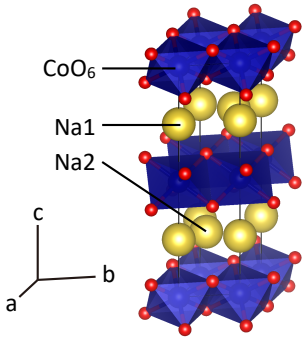

Figure 1. Crystal structure of $P2$-Na_xCoO_2. Large yellow spheres represent Na1 and Na2. Blue octahedra and small red spheres represent Co and O, respectively.

operating voltage of $\sim$ 2.5 V against Na in the sodium-ion secondary battery (SIB). From the point of view other than electrochemical properties, Na_xCoO_2 was intensively investigated due to its thermoelectoric properties[16], superconductivity[17], elecrtronic and magnetic properties[18, 19, 20]. Terasaki *et al.* reported lage thermoelectric power ($= 0.1$ mV/K at 300 K) in Na_xCoO_2 single crystal.[16] On the other hands, Tanaka *et al.* reported superconductivity at $T_C = 5$ K in $Na_xCoO_2 \cdot yH_2O$ ($x \sim 0.35, y \sim 1.3$).[19]

By means of first principles calculation, Hinuma *et al.*[12] have investigated the Na^+ ordering against the Na^+ concentration (x). They found characteristic ordering of Na^+ at $x = 1/2$, 5/9, 3/5, 2/3, 5/7, 10/13, 13/16, 16/19, and 18/21. In this sense, Na_xCoO_2 is expected to show the phase separation (PS) into $Na_{x_i}CoO_2$ and $Na_{x_{i+1}}CoO_2$ during the Na^+ intercalation process as

$$Na_{x_i}CoO_2 + (x_{i+1} - x_i)\left(Na^+ + e^-\right) \rightarrow Na_{x_{i+1}}CoO_2, \tag{2}$$

where x_i is the x value at respective single phase. Within the framework of the PS model, ΔS_{solid} is simply expressed as

$$\Delta S_{\text{solid}} = \frac{S(x_{i+1}) - S(x_i)}{x_{i+1} - x_i}. \tag{3}$$

Consistently with the calculation, Berthelot *et al.* reported a phase diagram of $P2$-Na_xCoO_2 and nine single-phases between $x = 0.5$ and 0.9 at room temperature.[13] Among them, the $x = 1/2$ and 2/3 phases are intensively investigated and superstructures arising from sodium orderings are proposed[21, 22].

In this paper, we experimentally determined α of $P2$-type Na_xCoO_2 against the Na^+ concentration (x). The solid component (α_{solid}) of α scatters from -0.18 mV/K to 0.64 mV/K. The PS model cannot reproduce the x-dependence even qualitatively. We interpreted the unexpected disagreement in terms of the residual configuration entropy in the pseudo-disordered region between the Na^+ ordered phases.

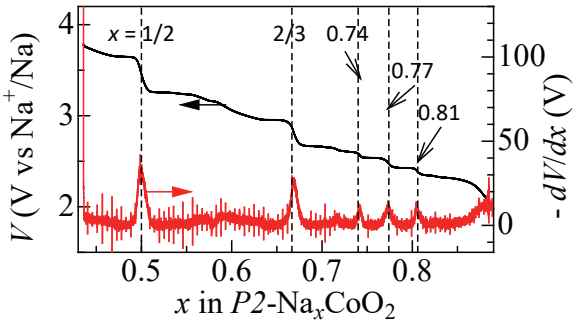

Figure 2. Discharge curve (black curve) of Na_xCoO_2 and its x-derivative. The discharge curve was obtained at the first cycle.

2. EXPERIMENTS

2.1. Sample preparation

Polycrystalline sample of $P2$-$Na_{0.7}CoO_2$ was prepared by solid state reaction. Na_2O_3 and Co_3O_4 were mixed in a 105 : 100 atomic ratio and calcined at 800 °C in air for 40 hours. To avoid hydration, the compound was kept in vacuum immediately after the calcination. X-ray powder diffraction (XRD) measurements were performed at the BL02B2 beamline of SPring-8 with one-dimensional semiconductor detector (MYTHEN, Dectries Ltd.). The samples were finely ground and placed in ϕ0.3 mm glass capillaries. The wavelength of the X-rays (= 0.70086 Å) was calibrated by the cell parameter of a standard CeO_2 powder. The XRD patterns were analyzed by the Rietveld method with a hexagonal model ($P6_3/mmc$; $Z = 2$). Lattice constants are $a = 2.8260(2)$ Å, $b = 10.976(1)$ Å. No traces of impurities nor secondary phases were observed.

2.2. Electrochemical measurement

The measurement of the discharge curve was performed with a potentiostat (Hokuto Denko Co. Ltd.) using a beaker-type two-pole cell. The cathode, anode, and electrolyte were the $P2$-$Na_{0.7}CoO_2$ electrode, sodium metal, and propylene carbonate (PC) containing 1 mol/L $NaClO_4$, respectively. To obtain the $P2$-$Na_{0.7}CoO_2$ electrode, a mixture of sample powder, ketchen black (KB), and polyvinylidene difluoride (PVDF) in 8 : 1 : 1 weight ratio was pasted on an Al foil. The active area of the electrode was about 0.4 cm^2.The cut-off voltage was from 2.0 V to 3.8 V and charge/discharge rate was 0.1 C. The measurement was performed under Ar atmosphere in an Ar filled glove box.

Figure 2 shows the discharge curve (black curve) of $P2$-Na_xCoO_2 and its x-derivative (dV/dx; red curve). The overall behavior is consistent with the data reported by Delmas *et al.*[11] Discontinuous drops are observed at $x = 1/2$, 2/3, 0.74, 0.77, and 0.81 in the discharge curve. These concentrations are ascribed to the Na^+ ordered phases proposed by GGA first principles calculations.[12] The $x = 0.77$ and 0.81 drops

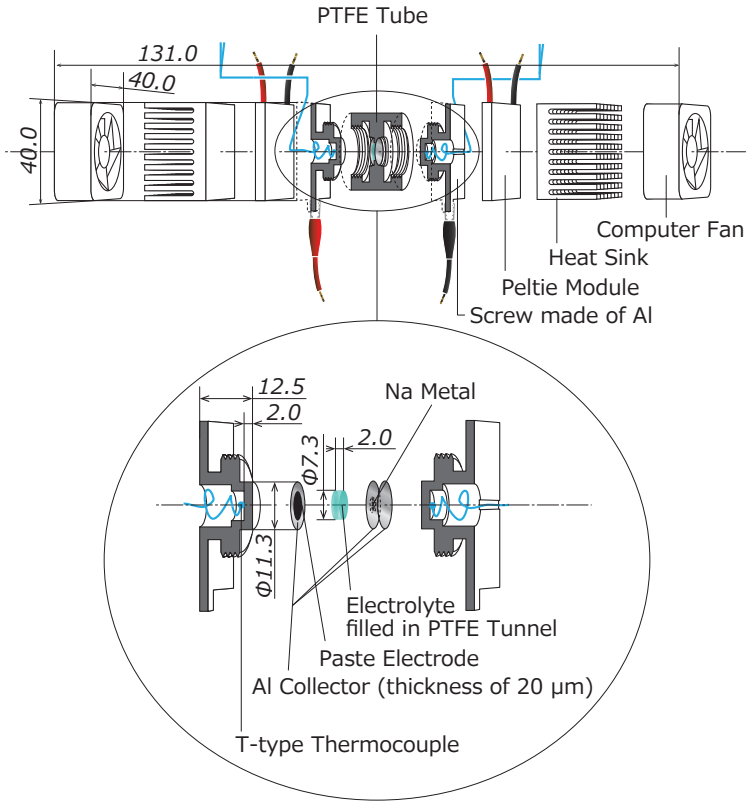

Figure 3. Illustration of specially-designed thermocell. Scales are in mm units.

can be ascribed to the 10/13- and 13/16- phases.[12] The exception is that the $x = 0.74$ drop could be attributed to a metastable crossover point where the Na1 sites start to form triplets rather than being isolated. Experimentally, the chemically-synthesized $Na_{0.5}CoO_2$ ($x = 1/2$)[23] and $Na_{0.67}CoO_2$ ($x = 2/3$)[24] are reported to show superlattice reflections related to the Na^+ ordering.

2.3. Determination of α

The α value of $P2$-Na_xCoO_2 was precisely determined with use of specially-designed thermocell (Fig. 3). The electrolyte was filled in a ϕ7.3 mm polytetrafluoroethylene (PTFE) tube. The both ends are sealed with the Al pedestals, on which Na metal and the paste electrode are attached as anode and cathode, respectively. The two electrodes were placed strictly parallel with a distance of 2 mm, which causes pseud one-dimensional thermal gradient within the electrolyte solution. The temperature of cathode (T) and anode (T_{anode}) are monitored with T-type thermocouples. The thermocouples are attached at the screws at a distance of 2 mm from the electrode-electrolyte interfaces. T and T_{anode} are independently controlled with Peltier modules attached at the bottom of the screws.

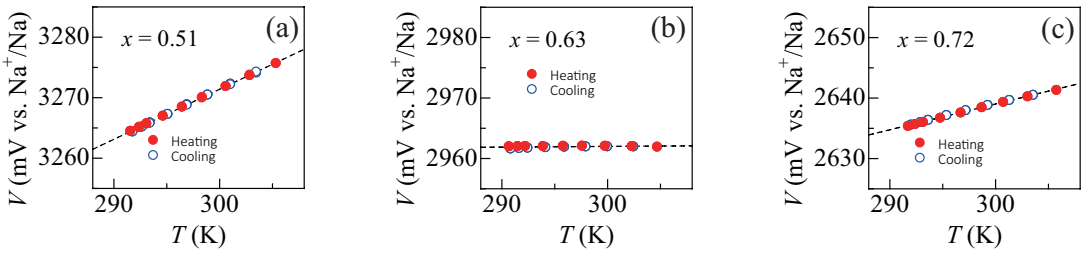

Figure 4. Temperature dependence of V of Na_xCoO_2: (a) $x = 0.51$, (b) 0.63, and (c) 0.72. Open and closed symbols represent that the data was obtained in the heating and cooling runs, respectively. Straight lines are results of least-squares fittings.

In the measurements, the anode temperature (T_{anode}) was kept at the initial temperature with a precision of 0.06 K or less. The cathode temperature (T) was precisely controlled with a Peltier module. The redox potential (V) of $P2$-Na_xCoO_2 versus the sodium metal was carefully measured against T under the open circuit condition. The x value was controlled by discharge process with constant current of 11.4 μA/cm^2 (0.1 C). In order to make $P2$-Na_xCoO_2 reach perfect thermal equilibrium, the measurement at each x was carried out at interval of 2 hours or more.

3. FIRST PRINCIPLES CALCULATIONS

To evaluated the solid component ($\alpha^{\mathrm{PS}}_{\mathrm{solid}}$) of α, S was calculated in the temperature range from 0 K to 500 K for the four ordered phases at $x = 1/2$, 2/3, 10/13, and 13/16.[12] First principles calculations were conducted using the projector augmented-wave method as implemented in the VASP code.[25, 26] For the calculation of Na_xCoO_2 and Na, the PBE functional[27] was used. For the calculation of Li, the PBEsol functional[28] was used. The calculation at a constant pressure of 0.1 MPa were performed using the quasi-harmonic approximation[29] as implemented in the phonopy code.[30]

4. RESULTS

4.1. x-dependence of α

Figure 4 shows temperature dependence of V of Na_xCoO_2: (a) $x = 0.51$, (b) 0.63, and (c) 0.72. Open and closed symbols represent that the data was obtained in the heating and cooling runs, respectively. Both the data points are almost overlapped, indicating that the data are free from temperature gradient nor the sample deterioration. At (a) $x = 0.51$, V linearly increases with T. α (= 0.83 mV/K) was evaluated by least-squares fitting, as indicated by broken straight line. At (b) $x = 0.63$, V is nearly independent of T. α (= 0.01 mV/K) was evaluated by least-squares fitting. At (c) $x = 0.72$, V linearly increases with T again. α (= 0.43 mV/K) was evaluated by least-squares fitting.

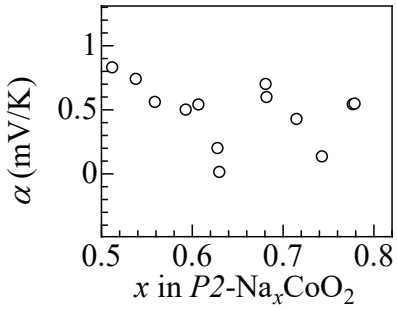

Figure 5. Temperature coefficient (α) of redox potential of Na_xCoO_2 against x.

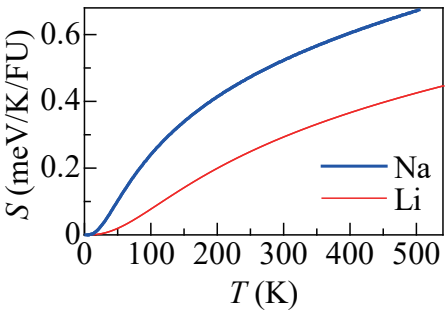

Figure 6. Temperature dependence of calculated entropy (S) for Li (red curve) and Na (blue curve).

Figure 5 shows thus determined α of $P2$-Na_xCoO_2 against x. α scatters from 0.0 mV/K to 0.9 mV/K. For example, α steeply decreases from 0.83 mV/K at $x = 0.51$ to 0.01 mV/K at $x = 0.63$. Such a steep reduction of α in $P2$-Na_xCoO_2 makes sharp contrast with the nearly constant ($= 0.9$ mV/K) behavior of α in Li_xFePO_4.[8]

4.2. Electrolyte component ($\alpha_{\mathrm{electrolyte}}$)

As described in introduction, ΔS can be divided into the components due to electrode solid material ($\Delta S_{\mathrm{solid}}$) and electrolyte ($\Delta S_{\mathrm{electrolyte}}$).[7] We note that $\Delta S_{\mathrm{electrolyte}}$ is expected to strongly depend on the solvent and ion species, because the major factors of $\Delta S_{\mathrm{electrolyte}}$ are the desolvation and extraction of the ion. For convenience of explanation, we will divide α into solid ($\alpha_{\mathrm{solid}} = \Delta S_{\mathrm{solid}}/e$) and electrolyte ($\alpha_{\mathrm{electrolyte}} = \Delta S_{\mathrm{electrolyte}}/e$) components.

Here, let us evaluate $\alpha_{\mathrm{electrolyte}}$ ($= \alpha - \alpha_{\mathrm{solid}}$) concerning to Li^+ and Na^+. Fukuzumi *et al.*[7] reported α for Li^+ and Na^+ in several solvents, *i.e.*, ethylene carbonate (EC) / diethyl carbonate (DEC), γ-butyrolactone (GBL), PC, and 1,2-dimethoxyethane (DME). On the other hand, α_{solid} is evaluated by first principles calculation. Figure 6 shows temperature dependence of S for Li (red curve) and Na (blue curve). In both the cases, S monotonously increases with temperature. S reaches 0.29 meV for Li and

Table 1. Solid ($\alpha_{\rm solid}$) and electrolyte ($\alpha_{\rm electrolyte}$) componets of α ($= {\rm d}V/{\rm d}T$) for Li^+ and Na^+ in several solvents, *i.e.*, ethylene carbonate (EC) / diethyl carbonate (DEC), γ-butyrolactone (GBL), propylene carbonate (PC), 1,2-dimethoxyethane (DME). $\alpha_{\rm solid}$ is evaluated by the entropy (S) of Li and Na. α is cited from literature.[7]

Ion species	Solute	Solvent	α (mV/K)	$\alpha_{\rm solid}$ (mV/K)	$\alpha_{\rm electrolyte}$ (mV/K)
Li^+	1M $LiClO_4$	EC/DEC	0.76	0.29	0.47
Li^+	1M $LiClO_4$	GBL	0.88	0.29	0.59
Na^+	1M $NaClO_4$	EC/DEC	0.77	0.52	0.25
Na^+	1M $NaClO_4$	GBL	0.73	0.52	0.21
Na^+	1M $NaClO_4$	PC	0.71	0.52	0.19
Na^+	1M $NaClO_4$	DME	1.70	0.52	1.18

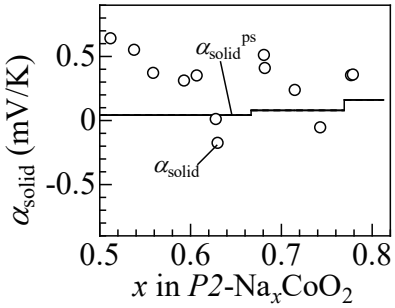

Figure 7. Solid component ($\alpha_{\rm solid} = \alpha - \alpha_{\rm electrolyte}$) of α of Na_xCoO_2 against x. The solid line represents calculated $\alpha_{\rm solid}^{\rm PS}$.

0.52 meV for Na at 300 K. These S values are consistent with the experiment.[31] In Table 1, we summarizes α, $\alpha_{\rm solid}$, and $\alpha_{\rm electrolyte}$.

4.3. x-dependence of solid component ($\alpha_{\rm solid}$)

Figure 7 shows solid component ($\alpha_{\rm solid} = \alpha - \alpha_{\rm electrolyte}$) of α of Na_xCoO_2 against x. Here, let us evaluate temperature coefficient of redox potential ($\alpha_{\rm solid}^{\rm PS}$) within the framework of the PS model (Eq. 2). The discharge curve (Fig. 2) suggests formation of the single phases at $x = 1/2$, 2/3, 0.74, 0.77, and 0.81. Among then, the 1/2-, 2/3-, 0.77-, and 0.81-phases can be ascribed to the 1/2-, 2/3, 10/13-, and 13/16-phase proposed by first principles calculation.[12] Then, $\Delta S_{\rm solid}$ is simply expressed as Eq. 3. Figure 8 shows temperature dependence of calculated $S(x)$ for Na_xCoO_2 at $x = 1/2$, 2/3, 10/13, and 13/16 per formula unit. $S(x)$ at 300 K are 0.6457, 0.6527, 0.6608, 0.6678 meV/K at $x = 1/2$, 2/3, 10/13, and 13/16, respectively. Solid line in Fig. 7 represents $\alpha_{\rm solid}^{\rm PS}$. The calculation cannot reproduce the x-dependence of $\alpha_{\rm solid}$ even qualitatively, especially, the steep reductions in $\alpha_{\rm solid}$ from $x = 0.51$ to 0.63 and from $x = 0.68$ to 0.74. We note that this unexpected disagreement should be ascribed to the PS model itself, because

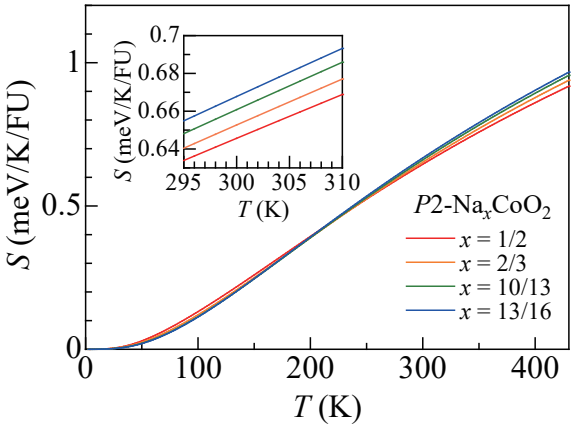

Figure 8. Temperature dependence of calculated entropy (S) for Na_xCoO_2 at $x = 1/2$, 2/3, 10/13, and 13/16. The inset shows magnified data.

we cannot reproduce the steep reduction even if we use another set of $S(x_i)$.

5. DISCUSSSION

What is the origin of the unexpected disagreement between experientially-obtained $\alpha_{\rm solid}$ and $\alpha_{\rm solid}^{\rm PS}$? We consider that the answer is in the phase boundary between the two Na^+ ordered phases. Figure 9(a) schematically shows the phase boundary between 0- and 1-phases. Such a phase boundary actually exists in Li_xFePO_4.[32] In this case, Li^+ intercalation takes place at the interface area.[32, 33] Important point is that the Li^+ intercalation at the interface area moves the phase boundary to the left side. We call such a boundary as "mobile" boundary. The situation is completely different in the phase boundary between 1/2- and 2/3-phases, as schematically shown in Fig. 9(b). Similar to the case of "mobile" boundary, Li^+ intercalation is considered to take place at the interface area. The Li^+ intercalation, however, cannot move the phase boundary, because addition of Na^+ on the 1/2-phase cannot produce the 2/3-type ordering. We call such a boundary as "immobile" boundary.

Nevertheless, the Na^+ intercalation and consequent phase transformation takes place in the actual Na_xCoO_2 system. Most probable scenario for the phase transformation is formation of the pseudo-disordered region between the 1/2- and 2/3-phases, in which the Na^+ ordering gradually changes from the 1/2- to 2/3-types. In such a pseudo-disordered region, the Na^+ migration is possible to move the phase boundary to the left side. Here, let us phenomenologically include the effect of the configuration entropy ($S_{\rm solid}^{\rm cf}$) in the pseudo-disordered region. Exact treatment of such a region, however, is difficult due to the residual correlation between Na^+. So, we crudely approximate $S_{\rm solid}^{\rm cf}$ in the disorder limit as

$$S_{\rm solid}^{\rm cf} = k_{\rm B}\ln\frac{(x_{i+1}-x_i)!}{(x-x_i)!\,(x_{i+1}-x)!}. \tag{4}$$

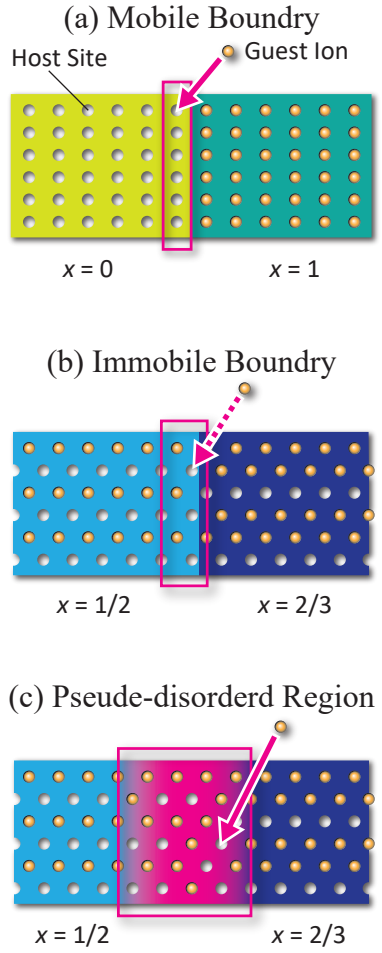

Figure 9. (a) Illustration of mobile phase boundary between the 0- and 1-phases, as exemplified by Li_xFePO_4. (b) Illustration of immobile phase boundary between the 1/2- and 2/3-phases, as exemplified by Na_xCoO_2. (c) Illustration of pseudo-disordered region between the 1/2- and 2/3-phases. The ordering patterns are simplified for inconvenience of explanation.

Then, the configuration component ($\alpha^{\rm cf}_{\rm solid}$) of α is given by

$$\alpha^{\rm cf}_{\rm solid} = \frac{1}{e}\frac{\partial S^{\rm cf}_{\rm solid}}{\partial x} = \frac{1}{e}k_{\rm B}\ln\frac{x_{i+1}-x}{x-x_i}. \tag{5}$$

The effective value ($\alpha^{\rm PS+cf}_{\rm solid}$) of α in the pseudo-disordered region is phenomenologically expressed as

$$\alpha^{\rm PS+cf}_{\rm solid} = (1-\beta)\,\alpha^{\rm PS}_{\rm solid} + \beta\alpha^{\rm cf}_{\rm solid}, \tag{6}$$

where $\alpha^{\rm PS}_{\rm solid}$ is the phase separation component. β is a phenomenological parameter. Figure 10 shows the compression of $\alpha^{\rm PS+cf}_{\rm solid}$ and experimentally-obtained $\alpha_{\rm solid}$. The phenomenological model qualitatively reproduced the x-dependence of $\alpha_{\rm solid}$, including the steep reduction in $\alpha_{\rm solid}$ from $x = 0.51$ to 0.63 and from $x = 0.68$ to 0.74.

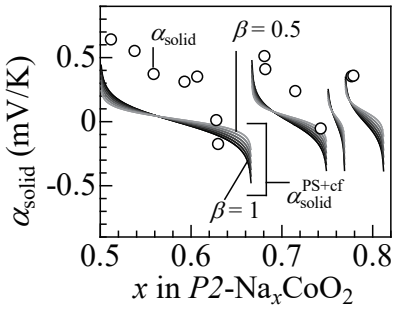

Figure 10. Solid component ($\alpha_{\rm solid} = \alpha - \alpha_{\rm electrolyte}$) of α of Na_xCoO_2 against x. Solid curve represents phenomenological model, $\alpha_{\rm solid}^{\rm PS+cf} = (1-\beta)\alpha_{\rm solid}^{\rm PS} + \beta\alpha_{\rm solid}^{\rm cf}$, where $\alpha_{\rm solid}^{\rm PS}$ and $\alpha_{\rm solid}^{\rm cf}$ are the phase separation and configuration components of α, respectively.

6. CONCLUSIONS

We experimentally determined α of $P2$-type Na_xCoO_2 against the Na^+ concentration (x). The solid component ($\alpha_{\rm solid}$) of α scatters from -0.18 mV/K to 0.64 mV/K. The PS model cannot reproduce the x-dependence even qualitatively. We interpreted the unexpected disagreement in terms of the residual configuration entropy in the pseudo-disordered region between the Na^+ ordered phases. Actually, a phenomenological model that partially include the configuration entropy qualitatively reproduced the experimtally-obtained $\alpha_{\rm solid}$. We believe that such a pseudo-disordered region between the ordered phases plays a significant role in the electrochemical processes of the battery materials.

Acknowledgments

This work was supported by JSPS KAKENHI (Grant Number JP17H0113). The synchrotron radiation experiments were performed at the BL02B2 of SPring-8 with the approval of the Japan Synchrotron Radiation Research Institute (JASRI) (Proposal Nos. 2018A1125 and 2017A1040).

[1] Seok Woo Lee, Yuan Yang, Hyun-Wook Lee, Hadi Ghasemi, Daniel Kraemer, Gang Chen, and Yi Cui. An electrochemical system for efficiently harvesting low-grade heat energy. *Nat. Commun.*, 5:3942, 2014.

[2] Yuan Yang, Seok Woo Lee, Hadi Ghasemi, James Loomis, Xiaobo Li, Daniel Kraemer, Guangyuan Zheng, Yi Cui, and Gang Chen. Charging-free electrochemical system for harvesting low-grade thermal energy. *Proceedings of the National Academy of Sciences*, 111(48):17011–17016, 2014.

[3] Jianjian Wang, Shien-Ping Feng, Yuan Yang, Nga Yu Hau, Mary Munro, Emerald Ferreira-Yang, and Gang Chen. “thermal charging” phenomenon in electrical double layer capacitors. *Nano Lett.*, 15(9):5784–5790, 2015.

[4] Yuya Fukuzumi, Kaoru Amaha, Hideharu Niwa, Wataru Kobayashi, and Yutaka Moritomo. Prussian blue analogues as promising thermal power generation materials. *Energy Technol.*, 6(10):1865–1870, 2018.

[5] Takayuki Shibata, Yuya Fukuzumi, Wataru Kobayashi, and Yutaka Moritomo. Thermal power generation during heat cycle near room temperature. *Appl. Phys. Express*, 11(1):017101, 2017.

[6] H. Julian Goldsmid. Springer-Verlag Berlin Heidelberg, 2010.

[7] Yuya Fukuzumi, Yoyo Hinuma, and Yutaka Moritomo. Thermal coefficient of redox potential of alkali metals. *J. Phys. Soc. Japan*, 87(5):055001, 2018.

[8] Yuya Fukuzumi, Yoyo Hinuma, and Yutaka Moritomo. Temperature coefficient of redox potential of lixfepo4. *AIP Adv.*, 8(6):065021, 2018.

[9] Hiroki Iwaizumi, Yusuke Fujiwara, Yuya Fukuzumi, and Yutaka Moritomo. The effect of 3d-electron configration entropy on the temperature coefficient of redoc potential in $co_{1-z}mn_z$ prussian blue analogues. *Dalton trans.*, 48:1964–1968, 2019.

[10] C Fouassier, G Matejka, JM Reau, and P Hagenmuller. On new bronze oxides of formula na_xcoo_2 ($x < 1$). system cobalt oxygen-sodium. *J. Solid State Chem*, 6:532, 1973.

[11] Claude Delmas, Jean-Jacques Braconnier, Claude Fouassier, and Paul Hagenmuller. Electrochemical intercalation of sodium in naxcoo2 bronzes. *Solid State Ion.*, 3/4:165–169, 1981.

[12] Yoyo Hinuma, Ying S Meng, and Gerbrand Ceder. Temperature-concentration phase diagram of p 2-na x coo 2 from first-principles calculations. *Phys. Rev. B*, 77(22):224111, 2008.

[13] Romain Berthelot, D Carlier, and Claude Delmas. Electrochemical investigation of the p2–na x coo 2 phase diagram. *Nat. Mater.*, 10(1):74, 2011.

[14] M Medarde, M Mena, JL Gavilano, E Pomjakushina, J Sugiyama, K Kamazawa, V Yu Pomjakushin, D Sheptyakov, B Batlogg, HR Ott, et al. 1d to 2d na+ ion diffusion inherently linked to structural transitions in na 0.7 coo 2. *Phys. Rev. Lett.*, 110(26):266401, 2013.

[15] Takayuki Shibata, Yuya Fukuzumi, Wataru Kobayashi, and Yutaka Moritomo. Fast discharge process of layered cobalt oxides due to high na+ diffusion. *Sci. Rep.*, 5:9006, 2015.

[16] Ichiro Terasaki, Yoshitaka Sasago, and Kunimitsu Uchinokura. Large thermoelectric power in naco 2 o 4 single crystals. *Physical Review B*, 56(20):R12685, 1997.

[17] Kazunori Takada, Hiroya Sakurai, Eiji Takayama-Muromachi, Fujio Izumi, Ruben A Dilanian, and Takayoshi Sasaki. Superconductivity in two-dimensional coo 2 layers. *Nature*, 422(6927):53, 2003.

[18] Michel Roger, DJP Morris, DA Tennant, MJ Gutmann, JP Goff, J-U Hoffmann, R Feyerherm, E Dudzik, D Prabhakaran, AT Boothroyd, et al. Patterning of sodium ions and the control of electrons in sodium cobaltate. *Nature*, 445(7128):631, 2007.

[19] Tomoaki Tanaka, Shin Nakamura, and Shuichi Iida. Observation of distinct metallic conductivity in naco2o4. *Japanese journal of applied physics*, 33(4B):L581, 1994.

[20] FC Chou, JH Cho, and YS Lee. Magnetic susceptibility study of hydrated and nonhydrated na x coo 2· y h 2 o single crystals. *Physical Review B*, 70(14):144526, 2004.

[21] HW Zandbergen, M Foo, Q Xu, V Kumar, and RJ Cava. Sodium ion ordering in na x coo 2: Electron diffraction study. *Physical Review B*, 70(2):024101, 2004.

[22] TA Platova, IR Mukhamedshin, H Alloul, AV Dooglav, and G Collin. Nuclear quadrupole resonance and x-ray investigation of the structure of na 2/3 coo 2. *Physical Review B*, 80(22):224106, 2009.

[23] Maw Lin Foo, Yayu Wang, Satoshi Watauchi, H W Zandbergen, Tao He, R J Cava, and N P Ong. Charge ordering, commensurability, and metallicity in the phase diagram of the layered na x co o 2. *Phys. Rev. Lett.*, 92(24):247001, 2004.

[24] T A Platova, I R Mukhamedshin, H Alloul, A V Dooglav, and G Collin. Nuclear quadrupole resonance and x-ray investigation of the structure of na 2/3 coo 2. *Phys. Rev. B*, 80(22):224106, 2009.

[25] G Kresse and J Furthmüller. G. kresse and j. furthmüller, phys. rev. b 54, 11169 (1996). *Phys. Rev. B*, 54:11169, 1996.

[26] Georg Kresse and D Joubert. From ultrasoft pseudopotentials to the projector augmented-wave method. *Phys. Rev. B*, 59(3):1758, 1999.

[27] John P Perdew, Kieron Burke, and Yue Wang. Generalized gradient approximation for the

exchange-correlation hole of a many-electron system. *Phys. Rev. B*, 54(23):16533, 1996.

[28] John P Perdew, Adrienn Ruzsinszky, Gábor I Csonka, Oleg A Vydrov, Gustavo E Scuseria, Lucian A Constantin, Xiaolan Zhou, and Kieron Burke. Restoring the density-gradient expansion for exchange in solids and surfaces. *Phys. Rev. Lett.*, 100(13):136406, 2008.

[29] Atsushi Togo, Laurent Chaput, Isao Tanaka, and Gilles Hug. First-principles phonon calculations of thermal expansion in ti 3 sic 2, ti 3 alc 2, and ti 3 gec 2. *Phys. Rev. B*, 81(17):174301, 2010.

[30] Atsushi Togo and Isao Tanaka. First principles phonon calculations in materials science. *Scr. Mater.*, 108:1–5, 2015.

[31] Raymond Chang. McGraw-Hill, 1998.

[32] C Delmas, M Maccario, L Croguennec, F Le Cras, and F Weill. Lithium deintercalation in lifepo4 nanoparticles via a domino-cascade model. *Nat. Mater.*, 7(8):665, 2008.

[33] Masamitsu Takachi and Yutaka Moritomo. In situ observation of macroscopic phase separation in cobalt hexacyanoferrate film. *Sci. Rep.*, 7:42694, 2017.